GEOPHYSICS, VOL. 81, NO. 4 (JULY-AUGUST 2016); P. E265–E277, 4 FIGS., 1 TABLE.
10.1190/GEO2015-0597.1

Approximate semianalytical solutions for the electromagnetic response of a dipping-sphere interacting with conductive overburden

Jacques K. Desmarais[1] and Richard S. Smith[2]

ABSTRACT

Electromagnetic exploration methods have important applications for geologic mapping and mineral exploration in igneous and metamorphic terranes. In such cases, the earth is often largely resistive and the most important interaction is between a conductor of interest and a shallow, thin, horizontal sheet representing glacial tills and clays or the conductive weathering products of the basement rocks (both of which are here termed the "conductive overburden"). To this end, we have developed a theory from which the step and impulse responses of a sphere interacting with conductive overburden can be quickly and efficiently approximated. The sphere model can also be extended to restrict the currents to flow in a specific orientation (termed the dipping-sphere model). The resulting expressions are called semianalytical because all relevant relations are developed analytically, with the exception of the time-convolution integrals. The overburden is assumed to not be touching the sphere, so there is no galvanic interactions between the bodies. We make use of the dipole sphere in a uniform field and thin sheet approximations; however, expressions could be obtained for a sphere in a dipolar (or nondipolar) field using a similar methodology. We have found that there is no term related to the first zero of the relevant Bessel function in the response of the sphere alone. However, there are terms for all other zeros. A test on a synthetic model shows that the combined sphere-overburden response can be reasonably approximated using the first-order perturbation of the overburden field. Minor discrepancies between the approximate and more elaborate numerical responses are believed to be the result of numerical errors. This means that in practice, the proposed approach consists of evaluating one convolution integral over a sum of exponentials multiplied by a polynomial function. This results in an extremely simple algorithmic implementation that is simple to program and easy to run. The proposed approach also provides a simple method that can be used to validate more complex algorithms. A test on field data obtained at the Reid Mahaffy site in Northern Ontario shows that our approximate method is useful for interpreting electromagnetic data even when the background is thick. We use our approach to obtain a better estimate of the geometry and physical properties of the conductor and evaluate the conductance of the overburden.

INTRODUCTION

Discrete conductor models have important applications for interpretation of data acquired using electromagnetic geophysical methods. Common models include the plate and sphere, which are commonly used for interpretation of borehole, ground, and airborne electromagnetic (BHEM, GEM, and AEM) data (Dyck et al., 1981; Dyck and West, 1984; Lamontagne et al., 1988; Macnae et al., 1998; Schaa, 2010; Smith and Wasylechko, 2012; Fullagar et al., 2015; Macnae, 2015; Vallée, 2015). In particular, the free-space discrete conductor model is attractive, especially in resistive environments such as large crystalline terranes due to the ease of computation (Annan, 1974; Smith and Lee, 2001). One of the simplest and most versatile of such models is the dipolar sphere in a uniform field, for which the secondary magnetic field can be calculated using a sum of exponentially decaying functions, where each term in the sum is related to a pole in the complex-frequency plane (Smith and Lee, 2001). This model provides a means to easily estimate the response of bodies of variable size, position, and conductivity. As well, the current at the sphere can be constrained to flow in a specified direction, so that computing the response of bodies of variable orientation is straightforward (Smith and Lee, 2002). This dipping-

Manuscript received by the Editor 3 November 2015; revised manuscript received 18 February 2016; published online 6 June 2016.
[1]Earth Sciences, University of Saskatchewan, Saskatoon, Saskatchewan, Canada. E-mail: jkd788@mail.usask.ca.
[2]Earth Sciences, Laurentian University, Sudbury, Ontario, Canada. E-mail: rssmith@laurentian.ca.

sphere model is used by Desmarais and Smith (2015a, 2015b) to develop GEM interpretation methods.

If the geology can be explained using a background or overburden that is conductive, free-space models may be inappropriate for modeling of electromagnetic data. Techniques exist for calculating the response of a discrete conductor interacting with other conductive bodies (Singh 1973; Lee, 1975, 1983; Ward and Hohmann, 1987; Bartel and Becker, 1988; Newman and Hohmann, 1988; Raiche and Sugeng, 1989; Walker and West, 1991). More specifically, the problem of a discrete conductor in a conductive medium is well-studied for electromagnetic applications in marine or other conductive environments (Wait, 1953; Song, 1993; San Filipo and Won, 2005; Shubitidze, 2011). Although these methods are generally based on integral forms of Maxwell's equations or solutions of Maxwell's equations in the frequency-wavenumber domain. Hence, they result in numerical implementations that are not used routinely for interpreting mineral exploration data.

Here, we are interested in the case of a discrete conductor embedded in a resistive environment because this is an important case for geologic mapping and mineral exploration in igneous and metamorphic terranes, where the background is resistive. In such cases, the interaction between the discrete conductor and a thin horizontal conductive sheet (representing an upper layer of glacial till or clay or a conductive weathering product) is often most important (Dyck and West, 1984; Xie et al., 1998). This problem is very relevant to mineral exploration and for such purposes, Liu and Asten (1993) have developed a theory for estimating the response of a wire loop interacting with conductive overburden. Their method assumes that the measurement at the receiver follows an ansatz, whereby the total field is written as a sum of the following form:

$$\boldsymbol{H} = \boldsymbol{H}_{\mathbf{ob}} + \sum_{n=1}^{\infty} \boldsymbol{H}_{\boldsymbol{n}} \approx \boldsymbol{H}_{\mathbf{ob}} + \boldsymbol{H}_{\mathbf{1}}, \tag{1}$$

where the first term $\boldsymbol{H}_{\mathbf{ob}}$ is the field from the overburden measured at the receiver, and higher-order terms are progressively weaker fields, which account for interaction between the overburden and the wire loop; $\boldsymbol{H}_{\mathbf{1}}$ is the field from the wire loop induced by $\boldsymbol{H}_{\mathbf{ob}}$; $\boldsymbol{H}_{\mathbf{2}}$ is the field from the overburden induced by $\boldsymbol{H}_{\mathbf{1}}$; $\boldsymbol{H}_{\mathbf{3}}$ is the field from the wire loop induced by $\boldsymbol{H}_{\mathbf{2}}$; and so on. Liu and Asten (1993) find that the total field $\boldsymbol{H}$ can be reasonably approximated using only $\boldsymbol{H}_{\mathbf{ob}}$ and $\boldsymbol{H}_{\mathbf{1}}$. The advantage of this approximation is that it results in calculations that are highly efficient, when compared to conventional methods. In fact, they find that the computation times were roughly 100 times faster than methods based on integral equations. However, one weakness of their model is the need to readjust empirically determined tuning parameters when the orientation and size of the wire loop varies.

Here, we aim to develop a theory for computing the time-domain electromagnetic response of a sphere under conductive overburden based on the ansatz introduced by Liu and Asten (1993). We envisage that this will provide the optimal method for estimating electromagnetic responses of discrete conductors in large metamorphic and igneous terranes, such as the Canadian Shield. The sphere is assumed not to be touching the overburden, so there can be no channeling of overburden currents into the sphere. We are interested in finding a fast and robust solution. To this end, we make use of the dipolar sphere in a uniform field model. However, generalization to a sphere in a dipolar (or nondipolar) field is straightforward. Here, no empirically derived tuning parameters are required and the dipping-sphere model is able to model plate-like bodies (Smith and Lee, 2001).

METHODOLOGY

Field of the overburden alone

Consider a transmitter consisting of a current-carrying loop. For AEM purposes, in which the height of the transmitter is much larger than the size of the loop, we can approximate the loop as a magnetic dipole. For GEM purposes, the transmitter could be represented using many magnetic dipoles (Desmarais and Smith, 2015a). The current at the transmitter is shut-off at time $t = 0$, at which point a time-varying magnetic field radiates everywhere in space. This magnetic field creates secondary currents in the overburden, which in turn generates a secondary-magnetic field. Here, we will assume that the overburden is sufficiently thin so that its electromagnetic properties can be described using a product of its conductivity and thickness (or conductance) σs. This is a good approximation in trying to describe the uppermost conductive layer because the width of this layer is generally much smaller than other system dimensions. The secondary field of the overburden $\boldsymbol{H}_{\mathbf{ob}}$ can be described using the receding-image solution of Grant and West (1965, p. 500):

$$\boldsymbol{H}_{\mathbf{ob}} = -\frac{u(t)}{4\pi}\left(\nabla_{\boldsymbol{rx}}\left\{\boldsymbol{m}_{\boldsymbol{tx}} \cdot \nabla_{\boldsymbol{tx}}\left[(r^x_{rx} - r^x_{tx})^2 + (r^y_{rx} - r^y_{tx})^2 + \left(r^z_{rx} \pm r^z_{tx} \pm \frac{2t}{\mu_o \sigma s}\right)^2\right]^{-\frac{1}{2}}\right\}\right), \tag{2}$$

where "·" is the dot product, $\boldsymbol{r}_{\boldsymbol{rx}} = [r^x_{rx}, r^y_{rx}, r^z_{rx}]$ is the receiver position and $\boldsymbol{r}_{\boldsymbol{tx}} = [r^x_{tx}, r^y_{tx}, r^z_{tx}] = [0, 0, d]$ is the transmitter position, in which d is the vertical distance from the transmitter to the overburden. The transmitter magnetic dipole moment vector is $\boldsymbol{m}_{\boldsymbol{tx}}$, $u(t)$ is the Heaviside-step-on function with $u(0) = 1$, μ_o is the vacuum permeability, $\nabla_{\boldsymbol{rx}}$ and $\nabla_{\boldsymbol{tx}}$ are the gradient operators acting on the receiver and transmitter coordinates, respectively. The plus and minus signs are used for receiver positions above or below the overburden. Here, we evaluate the gradients contained in $\boldsymbol{H}_{\mathbf{ob}}$ analytically. The resulting magnetic field expressions and its time derivative can be found in Appendix A (equations A-5a, A-5b, and A-5c).

Field of the sphere alone

Following Smith and Lee (2002), we will assume that the step response of a discrete conductor in free space $\boldsymbol{S}(t)$ can be written in the following form:

$$\boldsymbol{S}(t) = \boldsymbol{R}u(t)H(t), \tag{3}$$

where $\boldsymbol{R}$ is the inductive limit $(t \to 0)$ response and $H(t)$ is a dimensionless, analytic function characterizing the temporal decay of the currents induced at the conductor and follows the constraints:

$$\lim_{t\to 0^+} H(t) = 1 \tag{4a}$$

$$\lim_{t\to \infty} H(t) = 0. \tag{4b}$$

The impulse response $\boldsymbol{I}(t)$ is the time derivative of the step response:

$$\boldsymbol{I}(t) = \boldsymbol{R}\left\{\delta(t)H(t) + u(t)\frac{\partial H(t)}{\partial t}\right\}, \tag{5}$$

where $\delta(t)$ is the dirac-delta function. Smith and Lee (2002) were interested in the response in the off-time ($t > 0$), so they remove the delta function term because this term vanishes for $t > 0$:

$$\boldsymbol{K}(t) = \boldsymbol{R}u(t)\frac{\partial H(t)}{\partial t}. \tag{6}$$

For other purposes, if the term associated with the delta function were desired, it could be derived from $\boldsymbol{K}(t)$. Here, we wish to find the form of $\boldsymbol{S}(t)$. To do so, we can start from the formulation of Smith and Lee (2002). In their work, the magnetic field of the sphere in a dipole field is first described from the frequency-domain expression of Grant and West (1965, p. 518):

$$\mathcal{H}_i = \frac{m_j}{4\pi}\sum_{l=1}^{\infty}(X+iY)\frac{a^{2l+1}}{(rr_o)^{l+2}}F_i^j\{l, P_l^1(\cos\vartheta), P_l(\cos\vartheta)\}, \tag{7}$$

where $\mathcal{H}_i$ is the radial ($i = r$), latitudinal ($i = \vartheta$), or longitudinal ($i = \varphi$) component of the field; m_j is the jth component of the moment of the transmitter in spherical coordinates; a is the radius of the sphere r_o is the radial distance from the center of the sphere to the transmitter; r is the distance to the receiver; F_i^j is a function dependent on the index of summation l, and the Legendre coefficients P_l^1 and P_l. The only frequency-dependent term of equation 7 is given by the complex function $X + iY$ (Smith and Lee, 2002):

$$X + iY = \left[\frac{I_{\gamma+1}(ka)}{I_{\gamma-1}(ka)}\right], \tag{8}$$

where $\gamma = l + 1/2$ and $k = \sqrt{i\omega\mu_o\sigma_{sp}}$, for frequency ω and sphere conductivity σ_{sp}, and I are modified Bessel functions of the first kind. The time-dependent part of the impulse response in the off-time $\partial H(t)/\partial t$ is then given by the inverse Laplace transform of $X + iY$ (Smith and Lee, 2002):

$$\frac{\partial H(t)}{\partial t} = \mathcal{L}^{-1}\{X+iY\} = \frac{1}{2\pi i}\int_{c-i\infty}^{c+i\infty} e^{-\lambda^2 t/(\mu_o\sigma_{sp}a^2)}\left[\frac{J_{\gamma+1}(\lambda)}{J_{\gamma-1}(\lambda)}\right]\frac{2\lambda}{\mu_o\sigma_{sp}a^2}d\lambda, \tag{9}$$

where the integration variable is $\lambda = \sqrt{-i\omega\mu_o\sigma_{sp}a^2}$, J are Bessel functions of the first kind, and c is a variable along the real frequency axis, whose values exceeds the real part of all singularities of $X + iY$.

In the work of Smith and Lee (2002), this integral is evaluated using the residue theorem, which involves summing the contributions over simple poles of the integrand. Smith and Lee (2002) state that the integrand has poles at the zeros of $J_{\gamma-1}$, the first of which occurs at $\lambda = 0$. However, we find that the term related to the zero at $\lambda = 0$ leads to unphysical increases of $\boldsymbol{S}(t)$. We can evaluate the term in square brackets in equation 9 for $\lambda = 0$ using equation 9.1.7 of Abramowitz and Stegun (1965), which allows us to compute the value of the Bessel functions for small arguments:

$$\lim_{\lambda\to 0}\left[\frac{J_{\gamma+1}(\lambda)}{J_{\gamma-1}(\lambda)}\right] = \lim_{\lambda\to 0}\frac{\left(\frac{1}{2}\lambda\right)^{\gamma+1}\Gamma(\gamma)}{\left(\frac{1}{2}\lambda\right)^{\gamma-1}\Gamma(\gamma+2)} = 0, \tag{10}$$

where Γ is the Gamma function. Substituting equation 10 in 9, we realize that the integrand does not have a pole at $\lambda = 0$. However, according to the theorem of interlacing of zeros of Bessel functions in Watson (1944, p. 479), it is trivial to show that the integrand will have a simple pole for all other zeros of $J_{\gamma-1}(\lambda)$.

Then, following Smith and Lee (2002), the integral in equation 9 is evaluated using the residue theorem, which gives us a similar result:

$$\frac{\partial H(t)}{\partial t} = -\frac{4\gamma}{\mu_o\sigma_{sp}a^2}\sum_{k=1}^{\infty} e^{-\frac{\lambda_k^2 t}{(\mu_o\sigma_{sp}a^2)}}, \tag{11}$$

where now the λ_k are the non-null ($\lambda_k > 0$) zeros of $J_{\gamma-1}$. Equation 11 is similar to equation 22 of Smith and Lee (2002), except that here there is no $\lambda_k = 0$ term. We are interested in the case of a dipolar sphere in a uniform field, whose response is given by the first term in equation 7, associated with $l = 1$ and $\gamma = 3/2$ (Smith and Lee, 2001). In this case, λ_k are the non-null zeros of $J_{1/2} = \frac{\sin z}{\sqrt{\frac{1}{2}\pi z}}$, so we have $\lambda_k = n\pi$ for integers $n \in (1, \infty]$. The time-dependent part of the step response $H(t)$ is then obtained starting from the time integral of equation 11:

$$H(t) = -\frac{6}{\mu_o\sigma_{sp}a^2}\sum_{k=1}^{\infty}\int e^{-\frac{\lambda_k^2 t}{(\mu_o\sigma_{sp}a^2)}}dt = C + \sum_{k=1}^{\infty}\frac{6}{\lambda_k^2}e^{-\frac{\lambda_k^2 t}{(\mu_o\sigma_{sp}a^2)}} \tag{12}$$

where C is a constant of integration. From equation 4a, we have

$$1 = C + \sum_{k=1}^{\infty}\frac{6}{\lambda_k^2} = C + \frac{6}{\pi^2}\sum_{k=1}^{\infty}\frac{1}{k^2}. \tag{13}$$

The summation given in equation 13 was of interest to mathematicians in 17th–19th century and is known as the Basel problem in honor of Leonhard Euler, who found the exact sum to be $\pi^2/6$ (Ayoub, 1974). This gives us $C = 0$.

Following Smith and Lee (2002), the dipole moment induced at the sphere is then given by

$$\boldsymbol{m}_{\mathbf{sp}}(t) = 2\pi a^3 H(t)\boldsymbol{H}_{\boldsymbol{o}}, \tag{14}$$

where $\boldsymbol{H}_{\boldsymbol{o}}$ is the excitation field evaluated at the sphere. The observed magnetic field $\boldsymbol{S}(t)$ is then calculated as (Smith and Lee, 2002)

$$\boldsymbol{S}(t) = u(t)\frac{1}{4\pi r^3}\left[\frac{3\boldsymbol{m}_{\mathbf{sp}}(t)\cdot\boldsymbol{r}}{r^2}\boldsymbol{r} - \boldsymbol{m}_{\mathbf{sp}}(t)\right]. \tag{15}$$

Combined overburden and sphere response

The combined response of the sphere and overburden is approximated using an expression in the form given by equation 1. The first term in this expression $\boldsymbol{H}_{\mathbf{ob}}$ is given by equation 2 with $\pm$ replaced by a plus sign. The second term $\boldsymbol{H}_{\mathbf{1}}$ is the field of the sphere induced by the overburden. The field of the overburden is calculated again using the receding image solution, except that the coordinates of the sphere replace those of the receiver and $\pm$ is replaced by a minus sign.

In the Laplace domain, the first-order approximation for the induced moment at the sphere $\boldsymbol{m}_{\mathbf{1}}$ could be calculated using a multiplication of the field of the overburden with that of the sphere at the corresponding frequencies. In the time domain, an analogous quantity can be calculated using convolution. From Ampère's law, together with Faraday's and Ohm's laws in the quasistatic approximation, the induced moment at the sphere should be proportional to the time derivative of the excitation field $\boldsymbol{H}_{\mathbf{os}}$, which is the secondary field of the overburden evaluated at the sphere. This gives us

$$\boldsymbol{m}_{\mathbf{1}}(t) = -2\pi a^3 \frac{\partial \boldsymbol{H}_{\mathrm{os}}(t)}{\partial t} * u(t)H(t) \tag{16a}$$

$$\boldsymbol{m}_{\mathbf{1}}(t) = -2\pi a^3\left\{-\bar{\boldsymbol{H}}_{\mathrm{os}}(0)H(t) + \int_0^t \frac{\partial \bar{\boldsymbol{H}}_{\mathrm{os}}(\tau)}{\partial \tau}H(t-\tau)d\tau\right\}, \tag{16b}$$

where the negative sign out front is included for consistency with Maxwell's third equation, $\bar{\boldsymbol{H}}_{\mathrm{os}} = \boldsymbol{H}_{\mathrm{os}}/u(t)$ (see Appendix A, equation A-4) and τ is a convolution variable. The time derivative of $\boldsymbol{m}_{\mathbf{1}}$ can be calculated using the Leibniz integral rule:

$$\frac{\partial \boldsymbol{m}_{\mathbf{1}}(t)}{\partial t} = -2\pi a^3\left\{-\bar{\boldsymbol{H}}_{\mathrm{os}}(0)\frac{\partial H(t)}{\partial t} + \frac{\partial \bar{\boldsymbol{H}}_{\mathrm{os}}(t)}{\partial t} + \int_0^t \frac{\partial \bar{\boldsymbol{H}}_{\mathrm{os}}(\tau)}{\partial \tau}\frac{\partial H(t-\tau)}{\partial t}d\tau\right\}. \tag{17}$$

The actual field $\boldsymbol{H}_{\mathbf{1}}$ is then calculated using an equation similar to equation 15, except that the induced dipole moment is now $\boldsymbol{m}_{\mathbf{1}}(t)$ and the distance vector is now $\boldsymbol{r}_{\mathrm{os}}$. If the time derivative of the magnetic field is desired, it could be calculated using the time derivative of the moment given by equation 17. The third term $\boldsymbol{H}_{\mathbf{2}}$ in the approximation of the combined response is the field from the overburden induced by the sphere. The field $\boldsymbol{H}_{\mathbf{2}}$ can be calculated, again using the receding image solution, where the energizing moment is $\boldsymbol{m}_{\mathbf{1}}$ instead of the moment of the transmitter. As before, in the Laplace domain, the frequency dependence of $\boldsymbol{H}_{\mathbf{2}}$ could be obtained through multiplication of the frequency-dependent parts of the moment of the sphere with the secondary field of the overburden. This translates to a convolution in the time domain. Again from Maxwell's equations in the quasistatic approximation, the field $\boldsymbol{H}_{\mathbf{2}}$ is proportional to the time derivative of the field of the sphere evaluated at the overburden, which varies in time according to $\partial \boldsymbol{m}_{\mathbf{1}}(t)/\partial t$:

$$\boldsymbol{H}_{\mathbf{2}} = -\frac{u(t)}{4\pi}\left(\nabla_{\boldsymbol{rx}}\left\{\frac{\partial \boldsymbol{m}_{\mathbf{1}}(t)}{\partial t}\odot\nabla_{\mathrm{sp}}\left[(r_{rx}^x - r_{\mathrm{sp}}^x)^2 + (r_{rx}^y - r_{\mathrm{sp}}^y)^2 + \left(r_{rx}^z + r_{\mathrm{sp}}^z + \frac{2t}{\mu_o\sigma s}\right)^2\right]^{-\frac{1}{2}}\right\}\right), \tag{18}$$

where $\odot$ denotes a combination of the convolution and dot product operators ($\boldsymbol{a}\odot\boldsymbol{b} = a_1 * b_1 + a_2 * b_2 + a_3 * b_3$). Substituting equation 17 in equation 18, we get

$$\boldsymbol{H}_{\mathbf{2}} = \frac{-a^3}{2}\left(\nabla_{\boldsymbol{rx}}\left\{\int_0^t d\mathrm{T}\left[-\bar{\boldsymbol{H}}_{\mathrm{os}}(0)\frac{\partial H(\mathrm{T})}{\partial \mathrm{T}} + \frac{\partial \bar{\boldsymbol{H}}_{\mathrm{os}}(\mathrm{T})}{\partial \mathrm{T}} + \left\{\int_0^{t-\mathrm{T}}\frac{\partial \bar{\boldsymbol{H}}_{\mathrm{os}}(\tau)}{\partial \tau}\frac{\partial H(\mathrm{T}-\tau)}{\partial \mathrm{T}}d\tau\right\}\right.\right.\right.$$
$$\left.\left.\left.\cdot\nabla_{\mathrm{sp}}\left\{(r_{rx}^x - r_{\mathrm{sp}}^x)^2 + (r_{rx}^y - r_{\mathrm{sp}}^y)^2 + \left(r_{rx}^z + r_{\mathrm{sp}}^z + \frac{2(t-\mathrm{T})}{\mu_o\sigma s}\right)^2\right\}^{-\frac{1}{2}}\right]\right\}\right), \tag{19}$$

where T is a convolution variable. The analytical gradients contained in $\boldsymbol{H}_{\mathbf{2}}$ and its time derivative are evaluated in Appendix B.

Generalization to arbitrary waveforms

The response of the sphere-overburden system to excitation by an arbitrary current waveform pulse $\tilde{\boldsymbol{H}}$ can be calculated by convolving the step response $\boldsymbol{H}$ with the current waveform w or its time derivative:

$$\tilde{\boldsymbol{H}} = \int_{-P}^{0} w(\varpi)\boldsymbol{H}(t-\varpi)d\varpi, \tag{20}$$

where P is the pulse length and the waveform is assumed to be zero outside of the pulse. In BHEM, GEM, and AEM, the current waveform does not consist of one pulse, but of a series of alternating positive and negative (or bipolar repetitive) pulses. The effect of the previous pulses of the waveform is to reduce the amplitude of the field by factors proportional to the time constant of the decays. An analytical form for the amplitude reduction factors are given by Smith and Neil (2013) for responses consisting of a series of exponential decays (such as the response of the sphere alone). In principle, these factors would have a different analytical form for the combined

sphere-overburden response. However, for the models of interest to BHEM, GEM and AEM, the sphere is generally more conductive than the overburden. So, the residual magnetic field carried by the previous pulses of the waveform should be proportional to the field of the sphere alone, as the field of the overburden will have decayed away (see Figures 2 and 3). We can therefore safely approximate the amplitude reduction factors using those for the sphere alone:

$$\tilde{\boldsymbol{H}}(t) = \sum_{k=1}^{\infty} A(k) \int_{-P}^{0} w(\varpi) \boldsymbol{H_k}(t-\varpi) d\varpi \tag{21a}$$

$$A(k) = \left[1 + \exp\left\{\frac{-2\lambda_k^2}{\mu_o \sigma_{sp} a^2 f}\right\}\right]^{-1}, \tag{21b}$$

where f is the base frequency, $A(k)$ are the amplitude reduction factors of the bipolar repetitive waveform, and $\boldsymbol{H}_k$ are the spectral components of $\boldsymbol{H}$; (i.e., $\boldsymbol{H} = \sum_{k=1}^{\infty} \boldsymbol{H}_k$).

RESULTS

The equations presented in the previous section are solved in a MATLAB code. The only time-consuming parts of the computation is the evaluation of the convolution integrals. The convolution in equation 16b is evaluated using the MATLAB integral function, which is an implementation based on vectorized adaptive quadrature. The integral over τ in equation 20 is again evaluated using the MATLAB integral function and the integral over T is evaluated using the trapezoid integration method, as implemented in the *trapz* MATLAB function. The integral functions are called with the following arguments: a relative tolerance of 1E-5 and an absolute tolerance of 1E-20 A/m.

Synthetic models

To validate our solutions with regards to convergence of the sum in equation 1, we compare our results with those calculated using the sphere in a layered-earth solution of Vallée (2015). Unfortunately, the model used in the Vallée (2015) method is not identical to our model. There are some similarities in that the buried conductor is represented by dipoles. However, the sphere is assumed to be embedded in a conductive half-space and the overburden has a finite thickness. Furthermore, Vallée's layered-earth response is estimated using Hankel transforms and the solution is estimated in the frequency domain and transformed numerically to the time domain.

The geometry of the considered model, as well as its electromagnetic parameters are present in Figure 1. We convolved the step response with the time derivative of the MEGATEM waveform. The resulting signal was sampled in time according to the windows presented in Table 1. The height above ground of the transmitter was 120 m, the receiver was 56 m below and 125 m behind the transmitter. The dipole moment of the transmitter was 1.847300×10^6 Am^2 in the vertical direction. The length of the waveform pulse was 3.65 ms and its base frequency was 30 Hz.

The responses of the sphere and background alone are presented in Figure 2. Figure 2a shows the logarithm of the response of the infinitesimally thin overburden in the solid line and that of the layered-earth in the dotted-dashed line. Slight disparities are expected in these decays because of the inexactitude of the thin-sheet approximation (for the overburden) and because the host in the solution of Vallée (2015) does not have a zero conductivity (is not infinitely resistive). The agreement between our thin-sheet solution and the layered-earth solution appears to get slightly worse with increasing time. We attribute this to the noise floor in the numerical Hankel transforms used by the solution of Vallée (2015), which causes greater discrepancy when the signal is smaller (i.e., at late times). Figure 2b shows the response of the sphere using our formula in the solid line and that of the sphere using the solution of

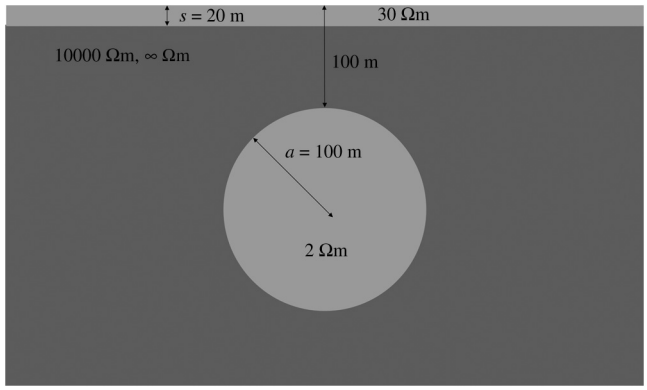

Figure 1. Geometry and electromagnetic parameters of the synthetic model used for the Vallée (2015) algorithm. In our algorithm, the thickness s is small, but the conductivity-thickness product is set to 0.666, the same value for the Vallée (2015) model. The other difference is that for the Vallée (2015) model, the host resistivity is 10,000 Ωm, but in our algorithm, we assume infinite resistivity.

Table 1. Window sampling times used in the synthetic model simulation.

Time after shut-off of the transmitter current (ms)
0.1546
0.2360
0.3337
0.4476
0.5778
0.7406
0.9440
1.1882
1.5137
1.9206
2.5309
3.3447
4.5654
6.1930
9.0143

Vallée (2015) in the dashed line. The differences of these two fields normalized by the peak at the associated windows are shown in Figure 2c. Here, the disparities are believed to be the result of numerical errors in the evaluation of the convolution with the system waveform (for both methods) and especially the evaluation of Hankel and Fourier transforms (for the method of Vallée, 2015). Again, the agreement is shown to get worse with time, likely a consequence of the constant noise in the numerical Hankel transforms for the method of Vallée (2015).

The combined responses are presented in Figure 3a. The Vallée (2015) solution is denoted by the dotted line, the second-order $(\boldsymbol{H}_{ob} + \boldsymbol{H}_1 + \boldsymbol{H}_2)$ solution is shown in the dotted-dashed line and the first-order $(\boldsymbol{H}_{ob} + \boldsymbol{H}_1)$ solution is shown in the solid line. The agreement between the fields calculated using our approach and that calculated using the approach of Vallée (2015) is good at early time but gets progressively worse with time, again likely because of the noise floor of the numerical Hankel transforms of the method of the Vallée (2015) algorithm, which becomes more apparent with decreasing delay time. Nonetheless, the good agreement in the first windows validates our approximate solution at early time. The remaining difference at early time is again most likely due to the thin-sheet approximation and numerical errors. Figure 3b shows the normalized difference of the first- and second-order solutions. The early windows are plotted in lighter shades and the later windows are plotted in darker shades. Figure 3b shows that the first- and second-order solutions converge to the same field at late time, which validates the approximate solution at late time.

The most important point is that the overburden and sphere response can be modeled approximately using our algorithm, and, hence, the physical and geometric properties of the overburden and the sphere can be estimated from the data. The small difference between the first- and second-order solutions suggests that in practice, good results can be obtained using only $\boldsymbol{H}_{ob}$ and $\boldsymbol{H}_1$. The Liu and Asten (1993) solution was shown to have a similar behavior

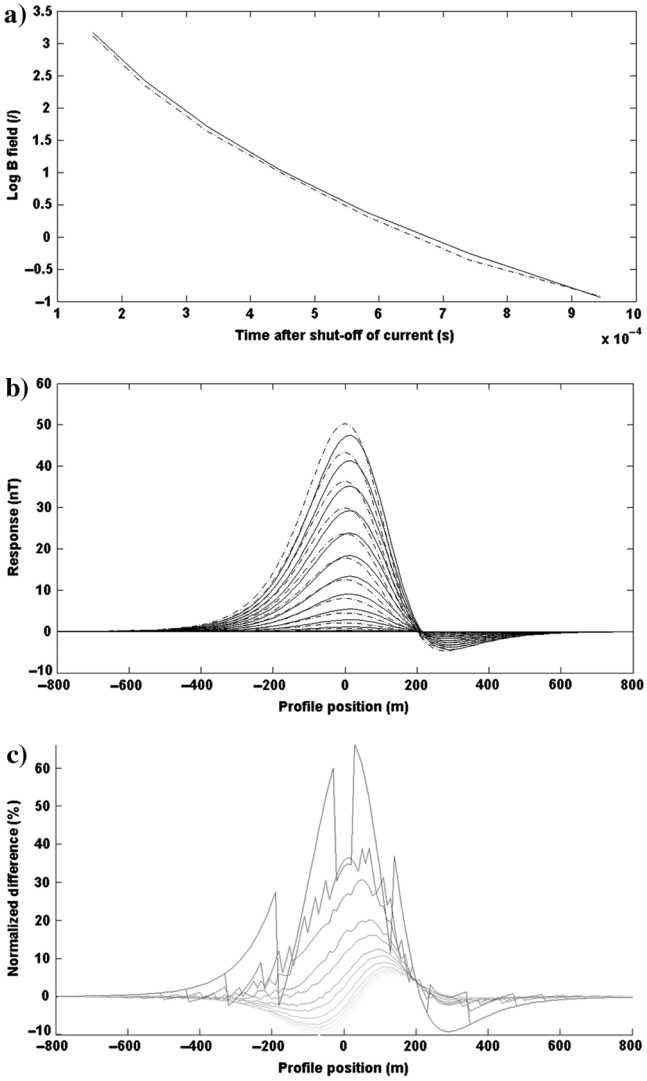

Figure 2. (a) Logarithm of the response of the overburden measured in nT (solid line) and the layered-earth (dashed line) for the first eight windows. (b) Secondary magnetic field of the dipole sphere in a uniform field using our solution (solid line) and the Vallée (2015) solution (dashed line). (c) Differences of the sphere's field calculated using our approach and that calculated using the approach of Vallée (2015), normalized by the peak at the corresponding window. The darker colors denote later times. It can be seen that the relative disagreement between these fields increases as a function of time and is attributed to the noise in the numerical Hankel transforms of the method of Vallée (2015).

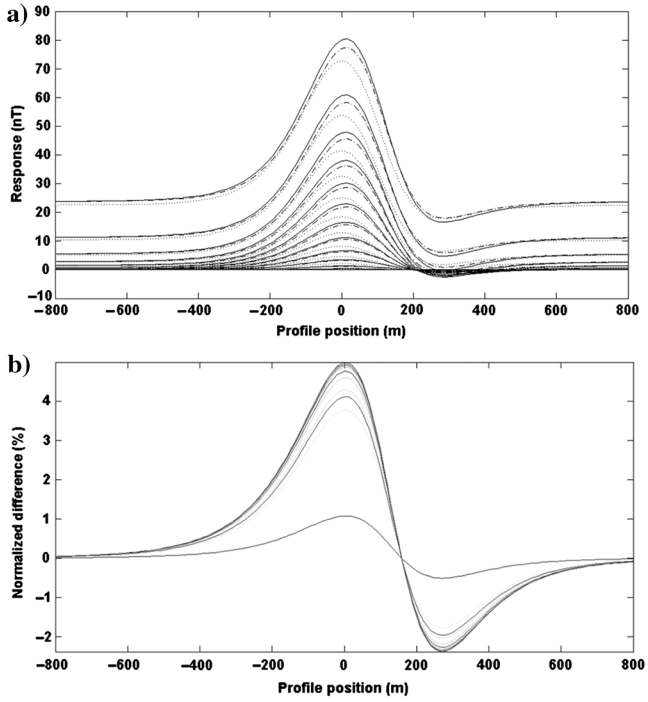

Figure 3. (a) Response of the sphere overburden system. The first-order field is in the solid line, the second-order field is in the dotted-dashed line and the solution obtained using the formula of Vallée (2015) is in the dotted line. The agreement between our solutions and that of Vallée (2015) is good for early time but gets worse with time as a result of the numerical Hankel transforms in the Vallée (2015) algorithm (see Figure 2). Nonetheless, this validates the approximation at early time. (b) Normalized difference between the first- and second-order fields. This plot shows that these fields converge to the same solution at late time, which validates the approximation at late time.

when compared to wire loop in a layered-earth models, in which disagreement was observed at early time between the layered-earth, first- and second-order solutions, but these converged to the same result at late time. It is not surprising that our solution has a similar behavior. The Vallée (2015) solution is limited to modeling currents that flow in a direction perpendicular to the excitation field at the sphere; our solution can restrict the currents to flow in a specific direction, which is necessary to explain field data, as we will see in the following section.

Test on field data from the Reid-Mahaffy site

To show some practical applications of our approach, we use our formula for forward modeling of an anomaly at line 15 of the Reid Mahaffy test site, Northern Ontario. This is the same anomaly discussed by Smith and Lee (2001, 2002), Smith and Salem (2007), Desmarais and Smith (2015c, 2016). This anomaly was modeled starting from the geometrical parameters obtained by Desmarais and Smith (2016) and the sphere conductivity-radius-squared (CRS) from Smith and Salem (2007). We use the dipping-sphere approach to model the response of an oriented body. This is done by projecting the first-order approximation to the dipole moment of the sphere $\boldsymbol{m_1}$ onto the normal $\boldsymbol{n}$ to the desired current flow path (Smith and Lee, 2002):

$$\tilde{\boldsymbol{m}}_1 = \hat{\boldsymbol{P}}\boldsymbol{m}_1 = \boldsymbol{n}\frac{\boldsymbol{n}\cdot\boldsymbol{m}_1}{n}. \tag{22}$$

The projection operator $\hat{\boldsymbol{P}}$ is time independent, so it can be applied after calculation of the integrals. After refinement of the parameters using a manual forward modeling procedure, we obtained a sphere position along the traverse line of 3300 m, a depth below ground to the center of the sphere of 230 m, a CRS of 6612 Sm, a strike of 90°, a dip of 85°, and an overburden conductance of 0.43 S. The resulting x- and z-component responses are shown in Figure 4a and 4b. The measured response is shown using the dashed line and the calculated response is shown using the solid line. Figure 4c and 4d shows the differences between the measured and calculated fields, normalized to the peak at the associated window. As can be seen from these figures, the agreement is not very good for the earliest and latest windows. There are two reasons for the poor early-time agreement: First, the overburden does not have a uniform thickness, as the x and z responses appear to be larger to the right. Second, the background is most likely thick. Therefore, a thin-sheet of uniform conductance is unable to model this complexity. Witherly et al. (2004) generate a map from drill information that shows that the overburden is approximately 60 m thick near this conductor; however, AEM inversions (without lateral constraints) on this line show that the overburden thickness is highly variable, changing very rapidly from less than 10 m to more than 40 m over very short distances (Vallée and Smith, 2009; Figure 4). However, the ground below the overburden is resistive, so the interaction with this background decays away quickly, and the agreement is good for the intermediate time windows.

At the latest windows, the amplitude of the anomaly is much lower and the data are corrupted by noise caused by swaying of the receiver coil. This is evident from the oscillation of the residual at late time in Figure 4c and 4d, as well as the oscillations in Figure 4e, which is a plot of the y-component of the anomaly. The y-component response is most sensitive to the offset to the traverse line of the conductor (Desmarais and Smith, 2016). Here, the amplitude of the y-component of this anomaly is low because the conductor lies below the traverse line and has a strike of 90°. However, as the receiver sways laterally, the offset from the receiver oscillates, which leads to the observed modulation of the amplitude in the y-component field (Desmarais and Smith, 2016). Nonetheless, we achieve good fits in the intermediate time windows, which are most dominated by the response of the discrete conductor. In mineral exploration and geologic mapping, the goal of applying AEM methods is often to extract information on the properties of the discrete conductor and the good intermediate-time agreement obtained with our approach suggests that we have achieved this goal at these delay times.

DISCUSSION

For the field example at the Reid-Mahaffy site, we obtained a depth different from the 200m obtained by Desmarais and Smith (2016). The depth of the sphere can be expected to change the time dependence of the combined response. If the depth of the sphere is infinite, then the combined response becomes the field of the overburden alone. Otherwise, the combined response will be a combination of the sphere response and the overburden response. These two situations create fields that have different time dependences, so the depth of the sphere affects the time dependence of the response. We have more confidence in the depth obtained here because of the formal inclusion of interaction with the overburden. The other advantage of this result over previous results is that the conductance of the overburden has been estimated in this work. Even better results could be obtained by implementing our formula in an inversion or automated interpretation algorithm.

We did not use the y-component because this component is weak in this instance and is dominated by noise. However, in other situations, the y-component could be used to estimate the strike or the lateral offset of the conductor. Although this is not critical in our situation because an estimate of the strike (90°) has already been obtained using the algorithm of Desmarais and Smith (2016).

The poor early-time agreement between the calculated and measured response at the Reid-Mahaffy site was caused by the uppermost conductive layer of variable conductance, which was not adequately modeled by a thin sheet of uniform conductance. However, the agreement for the intermediate delay times is much better because all other conductive features are well-represented using our model. If the electromagnetic properties of the uppermost conductive layer are of interest, then a method based on a thick sheet of variable conductance would be required. Otherwise, our approach appears to yield adequate results compared to the work of previous authors.

The resistivity of the host rock in the synthetic model was 10,000 Ωm for the layered-earth simulation and ∞ Ωm for the overburden simulation. The high resistivity value of the host rock was chosen to emulate free-space conditions, so that both solutions could be compared. Granted, these values are not representative of the host-rock resistivities encountered in all situations. However, the goal of this paper is not to validate the free-space approximation because the use of free-space methods is already a common practice in electromagnetic data interpretation, especially in the resistive environments of interest here (see the "Introduction" section). Our model assumes a free-space host below a thin conductive overbur-

den, which will be a better approximation than the free-space models with no overburden that are routinely used.

We have shown that an accurate description of the secondary-magnetic field of the sphere and overburden can be obtained using only the first-order interaction field. This means that the computation of a given Cartesian component of the response consists of simply evaluating one convolution integral over a sum of exponentials multiplied by a polynomial function. If the second-order interaction field were desired, then the calculation also requires the evaluation of a double-convolution integral over an integrand of similar analytical form. In either case, these methods are expected to outperform methods based on integral forms of Maxwell's equations or methods using analytical solutions of Maxwell's equations in the frequency-wavenumber domain (such as the method of Vallée, 2015). For a given Cartesian component of the secondary-magnetic field response, the Vallée (2015) algorithm calculates the field in the frequency-space domain by taking six Hankel transforms over integrands containing special functions such as Hankel and Bessel functions, as well as their first-, second- and third-order spatial numerical derivatives. The solution is then transformed to the space-time domain by using a 2D digital cosine transform, which results in an algorithmic implementation that is much more complex than our approach. The Vallée (2015) method has been implemented in a computer program that is the property of the Compagnie Générale Géophysique, and cannot be run by us or others in the geophysical community. So, we cannot directly compare execution times of both algorithms because they cannot be run on similar machines and in a similar programming language. It is also difficult to compare the cost of both algorithms based on floating point operations because the accuracy at which the integral transforms are calculated in Vallée (2015) and using our adaptive quadrature approach are dependent upon the geometry and electromagnetic properties of the considered model, as well as the delay time. However, when comparing their approximate-wire-loop algorithm with a more elaborate algorithm, Liu and Asten (1993) find a factor-of-100 improvement in execution time. Also noteworthy is that the algorithm

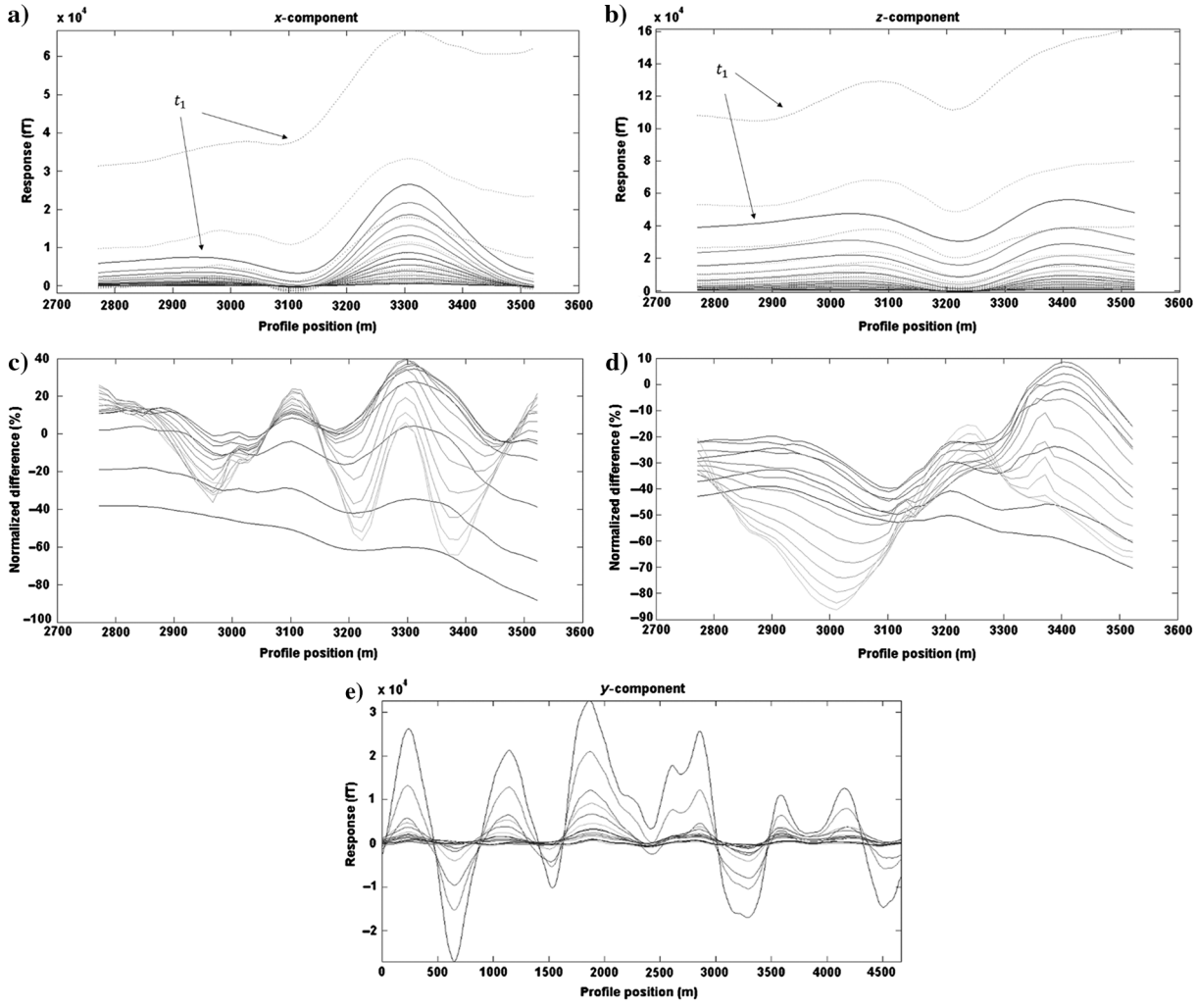

Figure 4. The (a) x- and (b) z-component responses at the Reid-Mahaffy site. The calculated responses are depicted using the solid lines, the measured responses are plotted using the dashed lines, and t_1 denotes the corresponding fields calculated at the first window. The (c) x- and (d) z-component normalized differences between the calculated field and the measured field. The (e) y-component response at the Reid-Mahaffy site.

of Vallée (2015) is for a layered-earth and if the background is not layered, it may yield erroneous results (Wolfgram et al., 1998; Reid et al., 2010). Admittedly, a similar error would occur with our method if the background is not represented well by a thin sheet. However, our method is expected to outperform a method based on layered-earths in the situation where the background is resistive and not layered, such as situations encountered in the large igneous and metamorphic terranes present in the Canadian Shield as well as other parts of North America. Also, our algorithm is able to model the electromagnetic response of oriented bodies in any arbitrary orientation, which is not possible in the algorithm of Vallée (2015). One major improvement over our approach against that of Liu and Asten (1993) is that our model does not require adjustment of empirical tuning of parameters while the properties of the discrete conductor vary.

CONCLUSION

We develop a theory from which the electromagnetic response of a dipping-sphere interacting with conductive overburden can be quickly and efficiently approximated. The method is especially useful in resistive environments, where the most important interaction is often between a conductor of interest and a thin horizontal and conductive sheet, which represents a layer of weathering products of the basement rocks, or surficial sediments such as glacial tills and clays. In the derivation of the step response of the sphere alone, we show that there is no term related to the first zero of the relevant Bessel function; however, there are terms related to all other zeros, which is a correction on the work of previous authors. A synthetic model test shows that the combined response can be reasonably approximated from the first-order perturbation of the overburden response. The discrepancies between our approximate solution and the full nondipping-sphere solution are most likely the result of numerical errors. Unlike the full nondipping solution, our model is able to account for current restricted to flow at a specific plane (the so-called dipping-sphere model). A test at the Reid-Mahaffy site in Northern Ontario shows that our approach is useful for interpretation of field data, even when the background is thick. Our parameters are in agreement with those of previous authors, and a better estimate of the depth, dip of current flow and CRS of the conductor, as well as the overburden conductance have been obtained. Tuning parameters such as those proposed by other authors are not required in our approach.

ACKNOWLEDGMENTS

We would like to acknowledge the assistance of J. Lemieux (formerly of CGG), who calculated the sphere in a layered-earth response using a CGG code written by M. A. Vallée. We thank C. Régis, M. A. Vallée, and two other anonymous reviewers for their suggestions, which helped improve this manuscript. Finally, we thank G. A. Desmarais Jr. for his grammatical suggestions.

LIST OF MATHEMATICAL SYMBOLS

$A(k)$	=	amplitude reduction factors of the transmitter waveform
a	=	radius of the sphere
c	=	variable along the real frequency axis
C	=	constant of integration
F_i^j	=	function dependent on l and the Legendre coefficients P_l^1 and P_l
f	=	waveform base frequency
$\boldsymbol{H}_{\mathbf{ob}}$	=	secondary-magnetic field of the overburden induced by the transmitter and evaluated at the receiver
$\tilde{\boldsymbol{H}}_{\mathbf{ob}}$	=	$\frac{\boldsymbol{H}_{\mathbf{ob}}}{u(t)}$
$\boldsymbol{H}_{\boldsymbol{n}}$	=	nth-order interaction field between the sphere and the overburden
$\boldsymbol{H}$	=	step response of the sphere-overburden system
$H(t)$	=	analytic function characterizing the decay of the magnetic field associated with the sphere
$\boldsymbol{H}_{\boldsymbol{o}}$	=	primary field of the transmitter
$\boldsymbol{H}_{\mathbf{os}}$	=	field of the overburden excited by the transmitter and evaluated at the sphere
$\tilde{\boldsymbol{H}}_{\mathbf{os}}$	=	$\frac{\boldsymbol{H}_{\mathbf{os}}}{u(t)}$
$\tilde{\boldsymbol{H}}$	=	combined sphere-overburden response to excitation by w
$\boldsymbol{H}_{\boldsymbol{k}}$	=	kth spectral component of $\boldsymbol{H} = \sum_{\boldsymbol{k}} \boldsymbol{H}_{\boldsymbol{k}}$
$\mathcal{H}_i$	=	radial $(i = r)$, latitudinal $(i = \vartheta)$ or longitudinal $(i = \varphi)$ component of the magnetic field of a sphere in a dipole field, expressed in the Laplace domain
$\boldsymbol{I}(t)$	=	impulse-response of the sphere
I_ν	=	modified Bessel functions of the first kind
i	=	$\sqrt{-1}$
J_ν	=	Bessel functions of the first kind
$\boldsymbol{K}(t)$	=	quadrature impulse response of the sphere
k	=	$\sqrt{i\omega\mu_o\sigma_{\mathrm{sp}}}$
$\mathcal{L}^{-1}$	=	inverse Laplace transform
l	=	index of summation for calculating $\mathcal{H}_i$
$\boldsymbol{m}_{\boldsymbol{tx}}$	=	dipole moment vector of the transmitter
m_j	=	jth spherical coordinate component of the moment of the transmitter
$\boldsymbol{m}_{\mathbf{sp}}(t)$	=	dipole moment vector of the sphere
$\boldsymbol{m}_{\mathbf{1}}(t)$	=	first-order approximation to the dipole moment of the sphere
$\tilde{\boldsymbol{m}}_{\mathbf{1}}(t)$	=	dipole moment of an oriented conductor
$\boldsymbol{n}$	=	normal to the plane containing the current flow path at the sphere
$\hat{\boldsymbol{P}}$	=	projection operator transforming the moment of the sphere into that of an oriented conductor
P	=	pulse length of the transmitter waveform
$\boldsymbol{R}$	=	inductive limit response of the sphere
$\boldsymbol{r}_{\boldsymbol{rx}}$	=	coordinates of the receiver
$\boldsymbol{r}_{\boldsymbol{tx}}$	=	coordinates of the transmitter
$\boldsymbol{r}_{\mathbf{os}}$	=	vector from the overburden to the sphere
$\boldsymbol{r}_{\mathbf{sp}}$	=	coordinates of the sphere
r_o	=	radial distance from the center of the sphere to the transmitter
r	=	radial distance from the center of the sphere to the receiver
$\boldsymbol{S}(t)$	=	step response of the sphere
t	=	time after shut-off of the transmitter current
$u(t)$	=	Heaviside-step-on function with $u(0) = 1$
w	=	waveform pulse weighting function
$X + iY$	=	frequency-dependent part of $\mathcal{H}_i$
Γ	=	gamma function
γ	=	$l + \frac{1}{2}$

$\delta(t)$ = Dirac delta function with nonzero argument for $\lim_{t\to 0^-}\delta(t)$
λ = $\sqrt{-i\omega\mu_o\sigma_{sp}a^2}$
λ_k = non-null zeros of $J_{\gamma-\frac{1}{2}}$
μ_o = vacuum permeability
σs = overburden conductance
σ_{sp} = conductivity of the sphere
τ, T, ϖ = convolution variables
ω = frequency of the field of the transmitter

APPENDIX A

ANALYTICAL GRADIENTS OF THE FIELD OF THE OVERBURDEN ALONE AND ITS TIME DERIVATIVE

From equation 2, we can write

$$\boldsymbol{H}_{\mathbf{ob}} = -\frac{u(t)}{4\pi}\left(\nabla_{\boldsymbol{rx}}\left\{\boldsymbol{m}_{\boldsymbol{tx}}\cdot\nabla_{tx}h^{-\frac{1}{2}}\right\}\right), \tag{A-1}$$

where h is the term in square brackets in equation 2. Evaluating the gradient of the coordinates of the overburden:

$$\boldsymbol{H}_{\mathbf{ob}} = -\frac{u(t)}{4\pi}\left(\nabla_{\boldsymbol{rx}}\left\{h^{-\frac{3}{2}}\left[m_x(r^x_{rx}-r^x_{tx}) + m_y(r^y_{rx}-r^y_{tx})\mp m_z\left(r^z_{rx}\pm r^z_{tx}\pm\frac{2t}{\mu_o\sigma s}\right)\right]\right\}\right) \tag{A-2}$$

where $\boldsymbol{m}_{\boldsymbol{tx}} = [m_x, m_y, m_z]$. We now evaluate the gradient over the receiver coordinates:

$$H^x_{\mathrm{ob}} = -\frac{u(t)}{4\pi}\left(-3h^{-\frac{5}{2}}(r^x_{rx}-r^x_{tx})\left[m_x(r^x_{rx}-r^x_{tx}) + m_y(r^y_{rx}-r^y_{tx})\mp m_z\left(r^z_{rx}\pm r^z_{tx}\pm\frac{2t}{\mu_o\sigma s}\right)\right] + h^{-\frac{3}{2}}m_x\right), \tag{A-3a}$$

$$H^y_{\mathrm{ob}} = -\frac{u(t)}{4\pi}\left(-3h^{-\frac{5}{2}}(r^y_{rx}-r^y_{tx})\left[m_x(r^x_{rx}-r^x_{tx}) + m_y(r^y_{rx}-r^y_{tx})\mp m_z\left(r^z_{rx}\pm r^z_{tx}\pm\frac{2t}{\mu_o\sigma s}\right)\right] + h^{-\frac{3}{2}}m_y\right), \tag{A-3b}$$

$$H^z_{\mathrm{ob}} = -\frac{u(t)}{2\pi\mu_o\sigma s}\left(\mp 3h^{-\frac{5}{2}}\left(r^z_{rx}\pm r^z_{tx}\pm\frac{2t}{\mu_o\sigma s}\right)\left[m_x(r^x_{rx}-r^x_{tx}) + m_y(r^y_{rx}-r^y_{tx})\mp m_z\left(r^z_{rx}\pm r^z_{tx}\pm\frac{2t}{\mu_o\sigma s}\right)\right] - h^{-\frac{3}{2}}m_z\right). \tag{A-3c}$$

The time derivative of the field of the overburden is now evaluated as

$$\frac{\partial \boldsymbol{H}_{\mathbf{ob}}}{\partial t} = u(t)\frac{\partial \bar{\boldsymbol{H}}_{\mathbf{ob}}}{\partial t} + \delta(t)\bar{\boldsymbol{H}}_{\mathbf{ob}}, \tag{A-4}$$

where $\bar{\boldsymbol{H}}_{\mathbf{ob}} = \boldsymbol{H}_{\mathbf{ob}}/u(t)$. This gives us

$$\frac{\partial H^x_{\mathrm{ob}}}{\partial t} = -\frac{u(t)}{4\pi}\left(\frac{15}{2}h^{-\frac{7}{2}}\frac{\partial h}{\partial t}(r^x_{rx}-r^x_{tx}) \times\left[m_x(r^x_{rx}-r^x_{tx}) + m_y(r^y_{rx}-r^y_{tx})\mp m_z\left(r^z_{rx}\pm r^z_{tx}\pm\frac{2t}{\mu_o\sigma s}\right)\right] + 3h^{-\frac{5}{2}}(r^x_{rx}-r^x_{tx})\frac{2m_z}{\mu_o\sigma s} - \frac{3}{2}h^{-\frac{5}{2}}\frac{\partial h}{\partial t}m_x\right) + \delta(t)\bar{H}^x_{\mathrm{ob}}, \tag{A-5a}$$

$$\frac{\partial H^y_{\mathrm{ob}}}{\partial t} = -\frac{u(t)}{4\pi}\left(\frac{15}{2}h^{-\frac{7}{2}}\frac{\partial h}{\partial t}(r^y_{rx}-r^y_{tx})\left[m_x(r^x_{rx}-r^x_{tx}) + m_y(r^y_{rx}-r^y_{tx})\mp m_z\left(r^z_{rx}\pm r^z_{tx}\pm\frac{2t}{\mu_o\sigma s}\right)\right] + 3h^{-\frac{5}{2}}(r^y_{rx}-r^y_{tx})\frac{2m_z}{\mu_o\sigma s} - \frac{3}{2}h^{-\frac{5}{2}}\frac{\partial h}{\partial t}m_y\right) + \delta(t)\bar{H}^y_{\mathrm{ob}}, \tag{A-5b}$$

$$\frac{\partial H^z_{\mathrm{ob}}}{\partial t} = -\frac{u(t)}{2\pi\mu_o\sigma s}\left(\pm\frac{15}{2}h^{-\frac{7}{2}}\frac{\partial h}{\partial t}\left(r^z_{rx}\pm r^z_{tx}\pm\frac{2t}{\mu_o\sigma s}\right)\left[m_x(r^x_{rx}-r^x_{tx}) + m_y(r^y_{rx}-r^y_{tx})\mp m_z\left(r^z_{rx}\pm r^z_{tx}\pm\frac{2t}{\mu_o\sigma s}\right)\right] - 3h^{-\frac{5}{2}}\frac{2}{\mu_o\sigma s}\left[m_x(r^x_{rx}-r^x_{tx}) + m_y(r^y_{rx}-r^y_{tx})\mp m_z\left(r^z_{rx}\pm r^z_{tx}\pm\frac{2t}{\mu_o\sigma s}\right)\right] \pm 3h^{-\frac{5}{2}}\left(r^z_{rx}\pm r^z_{tx}\pm\frac{2t}{\mu_o\sigma s}\right)\frac{2m_z}{\mu_o\sigma s} + \frac{3}{2}h^{-\frac{5}{2}}\frac{\partial h}{\partial t}m_z\right) + \delta(t)\bar{H}^z_{\mathrm{ob}}, \tag{A-5c}$$

where the time derivative of h is as follows:

$$\frac{\partial h}{\partial t} = \frac{\pm 4}{\mu_o\sigma s}\left(r^z_{rx}\pm r^z_{tx}\pm\frac{2t}{\mu_o\sigma s}\right). \tag{A-6}$$

APPENDIX B

ANALYTICAL GRADIENTS OF THE SECOND-ORDER INTERACTION FIELD AND ITS TIME DERIVATIVE

The first-order moment of the sphere $\boldsymbol{m}_1$ does not depend on the coordinates of the receiver. So, the analytical gradients of $\boldsymbol{H}_2$ are given by equations similar to equations A-3a–A-3c, with the moment of the transmitter replaced by $\boldsymbol{m}_1$, the coordinates of the transmitter replaced by those of the sphere, the $\mp$ replaced by a positive sign, and the $\pm$ replaced by a negative sign.

From the Leibniz integral rule, the time derivative of $\boldsymbol{H}_2$ reads

$$\frac{\partial \boldsymbol{H}_2}{\partial t} = \frac{1}{4\pi}\left(\nabla_{\boldsymbol{rx}}\left[\int_0^t\left\{\frac{\partial \boldsymbol{M}}{\partial t}\cdot\nabla_{\mathbf{sp}}h^{-\frac{1}{2}}\right\} + \left\{\boldsymbol{M}\cdot\nabla_{\mathbf{sp}}\left[-\frac{1}{2}h^{-\frac{3}{2}}\frac{\partial h}{\partial t}\right]\right\}d\mathrm{T}\right] + \nabla_{\boldsymbol{rx}}\left[\boldsymbol{M}\cdot\nabla_{\mathbf{sp}}h^{-\frac{1}{2}}\right]_{\mathrm{T}=t}\right), \tag{B-1}$$

where the following notations have been adopted as

$$\boldsymbol{M} = -2\pi a^3\left\{-\bar{\boldsymbol{H}}_{\rm os}(0)\frac{\partial H(\mathrm{T})}{\partial \mathrm{T}} + \frac{\partial \bar{\boldsymbol{H}}_{\rm os}(\mathrm{T})}{\partial \mathrm{T}} + \int_0^{t-\mathrm{T}} \frac{\partial \bar{\boldsymbol{H}}_{\rm os}(\tau)}{\partial \tau}\frac{\partial H(\mathrm{T}-\tau)}{\partial \mathrm{T}}\,d\tau\right\} \tag{B-2a}$$

$$\boldsymbol{M} = [M_x, M_y, M_z] \tag{B-2b}$$

$$h = \left[(r_{rx}^x - r_{\rm sp}^x)^2 + (r_{rx}^y - r_{\rm sp}^y)^2 + \left(r_{rx}^z - r_{\rm sp}^z - \frac{2(t-\mathrm{T})}{\mu_o\sigma s}\right)^2\right] \tag{B-3}$$

$$\frac{\partial \boldsymbol{M}}{\partial t} = -2\pi a^3 \frac{\partial \bar{\boldsymbol{H}}_{\rm os}(t-\mathrm{T})}{\partial (t-\mathrm{T})}\frac{\partial H(2\mathrm{T}-t)}{\partial \mathrm{T}} \tag{B-4}$$

$$\frac{\partial h}{\partial t} = -\frac{4}{\mu_o\sigma s}\left(r_{rx}^z - r_{\rm sp}^z - \frac{2(t-\mathrm{T})}{\mu_o\sigma s}\right). \tag{B-5}$$

We first evaluate the gradients over the sphere coordinates:

$$\begin{aligned}\frac{\partial \boldsymbol{H_2}}{\partial t} = \frac{1}{4\pi}\Bigg(&\nabla_{\boldsymbol{rx}}\Bigg[\int_0^t\Bigg\{h^{-\frac{3}{2}}\Bigg[\frac{\partial M_x}{\partial t}(r_{rx}^x - r_{\rm sp}^x) + \frac{\partial M_y}{\partial t}(r_{rx}^y - r_{\rm sp}^y) \\ &+ \frac{\partial M_z}{\partial t}\left(r_{rx}^z - r_{\rm sp}^z - \frac{2(t-\mathrm{T})}{\mu_o\sigma s}\right)\Bigg]\Bigg\} \\ &- \Bigg\{\frac{3M_x}{2}h^{-\frac{5}{2}}(r_{rx}^x - r_{\rm sp}^x)\frac{\partial h}{\partial t} + \frac{3M_y}{2}h^{-\frac{5}{2}}(r_{rx}^y - r_{\rm sp}^y)\frac{\partial h}{\partial t} \\ &+ \frac{3M_z}{2}h^{-\frac{5}{2}}\left(r_{rx}^z - r_{\rm sp}^z - \frac{2(t-\mathrm{T})}{\mu_o\sigma s}\right)\frac{\partial h}{\partial t} + \frac{2}{\mu_o\sigma s}h^{-\frac{3}{2}}\Bigg\}d\mathrm{T}\Bigg]\Bigg) \\ &+ \frac{1}{4\pi}\nabla_{\boldsymbol{rx}}\Bigg\{h^{-\frac{3}{2}}\Bigg[\left(\frac{\partial \bar{H}_{\rm os}^x(\mathrm{t})}{\partial \mathrm{t}} - \bar{H}_{\rm os}^x(0)\frac{\partial H(\mathrm{t})}{\partial \mathrm{t}}\right)(r_{rx}^x - r_{\rm sp}^x) \\ &+ \left(\frac{\partial \bar{H}_{\rm os}^y(\mathrm{t})}{\partial \mathrm{t}} - \bar{H}_{\rm os}^y(0)\frac{\partial H(\mathrm{t})}{\partial \mathrm{t}}\right)(r_{rx}^y - r_{\rm sp}^y) \\ &+ \left(\frac{\partial \bar{H}_{\rm os}^z(\mathrm{t})}{\partial \mathrm{t}} - \bar{H}_{\rm os}^z(0)\frac{\partial H(\mathrm{t})}{\partial \mathrm{t}}\right)(r_{rx}^z - r_{\rm sp}^z)\Bigg]\Bigg\},\end{aligned} \tag{B-6}$$

The gradient over the receiver coordinates is then evaluated:

$$\begin{aligned}\frac{\partial H_2^x}{\partial t} = \frac{1}{4\pi}\Bigg(&\Bigg[\int_0^t\Bigg\{-3h^{-\frac{5}{2}}(r_{rx}^x - r_{\rm sp}^x) \\ &\times\Bigg[\frac{\partial M_x}{\partial t}(r_{rx}^x - r_{\rm sp}^x) + \frac{\partial M_y}{\partial t}(r_{rx}^y - r_{\rm sp}^y) + \frac{\partial M_z}{\partial t} \\ &\times\left(r_{rx}^z - r_{\rm sp}^z - \frac{2(t-\mathrm{T})}{\mu_o\sigma s}\right)\Bigg] + h^{-\frac{3}{2}}\frac{\partial M_x}{\partial t}\Bigg\} \\ &-\Bigg\{-\frac{15M_x}{2}h^{-\frac{7}{2}}(r_{rx}^x - r_{\rm sp}^x)^2\frac{\partial h}{\partial t} + \frac{3M_x}{2}h^{-\frac{5}{2}}\frac{\partial h}{\partial t} \\ &-\frac{15M_y}{2}h^{-\frac{7}{2}}(r_{rx}^x - r_{\rm sp}^x)(r_{rx}^y - r_{\rm sp}^y)\frac{\partial h}{\partial t} \\ &-\frac{15M_z}{2}h^{-\frac{7}{2}}(r_{rx}^x - r_{\rm sp}^x)\left(r_{rx}^z - r_{\rm sp}^z - \frac{2(t-\mathrm{T})}{\mu_o\sigma s}\right)\frac{\partial h}{\partial t} \\ &-\frac{6}{\mu_o\sigma s}h^{-\frac{5}{2}}(r_{rx}^x - r_{\rm sp}^x)\Bigg\}d\mathrm{T}\Bigg]\Bigg) + \frac{1}{4\pi}\Bigg\{-3h^{-\frac{5}{2}}(r_{rx}^x - r_{\rm sp}^x) \\ &\times\Bigg[\left(\frac{\partial \bar{H}_{\rm os}^x(\mathrm{t})}{\partial \mathrm{t}} - \bar{H}_{\rm os}^x(0)\frac{\partial H(\mathrm{t})}{\partial \mathrm{t}}\right)(r_{rx}^x - r_{sp}^x) \\ &+ \left(\frac{\partial \bar{H}_{os}^y(\mathrm{t})}{\partial \mathrm{t}} - \bar{H}_{\rm os}^y(0)\frac{\partial H(\mathrm{t})}{\partial \mathrm{t}}\right)(r_{rx}^y - r_{\rm sp}^y) \\ &+ \left(\frac{\partial \bar{H}_{\rm os}^z(\mathrm{t})}{\partial \mathrm{t}} - \bar{H}_{\rm os}^z(0)\frac{\partial H(\mathrm{t})}{\partial \mathrm{t}}\right)(r_{rx}^z - r_{\rm sp}^z)\Bigg] \\ &+ h^{-\frac{3}{2}}\left(\frac{\partial \bar{H}_{\rm os}^x(\mathrm{t})}{\partial \mathrm{t}} - \bar{H}_{\rm os}^x(0)\frac{\partial H(\mathrm{t})}{\partial \mathrm{t}}\right)\Bigg\},\end{aligned} \tag{B-7a}$$

$$\begin{aligned}\frac{\partial H_2^y}{\partial t} = \frac{1}{4\pi}\Bigg(&\Bigg[\int_0^t\Bigg\{-3h^{-\frac{5}{2}}(r_{rx}^y - r_{\rm sp}^y)\Bigg[\frac{\partial M_x}{\partial t}(r_{rx}^x - r_{\rm sp}^x) + \frac{\partial M_y}{\partial t} \\ &\times(r_{rx}^y - r_{\rm sp}^y) + \frac{\partial M_z}{\partial t}\left(r_{rx}^z - r_{\rm sp}^z - \frac{2(t-\mathrm{T})}{\mu_o\sigma s}\right)\Bigg] + h^{-\frac{3}{2}}\frac{\partial M_y}{\partial t}\Bigg\} \\ &-\Bigg\{-\frac{15M_x}{2}h^{-\frac{7}{2}}(r_{rx}^x - r_{\rm sp}^x)(r_{rx}^y - r_{\rm sp}^y)\frac{\partial h}{\partial t} \\ &-\frac{15M_y}{2}h^{-\frac{7}{2}}(r_{rx}^y - r_{\rm sp}^y)^2\frac{\partial h}{\partial t} + \frac{3M_y}{2}h^{-\frac{5}{2}}\frac{\partial h}{\partial t} \\ &-\frac{15M_z}{2}h^{-\frac{7}{2}}(r_{rx}^y - r_{\rm sp}^y)\left(r_{rx}^z - r_{\rm sp}^z - \frac{2(t-\mathrm{T})}{\mu_o\sigma s}\right)\frac{\partial h}{\partial t} \\ &-\frac{6}{\mu_o\sigma s}h^{-\frac{5}{2}}(r_{rx}^y - r_{\rm sp}^y)\Bigg\}d\mathrm{T}\Bigg]\Bigg) + \frac{1}{4\pi}\Bigg\{-3h^{-\frac{5}{2}}(r_{rx}^y - r_{\rm sp}^y) \\ &\times\Bigg[\left(\frac{\partial \bar{H}_{\rm os}^x(\mathrm{t})}{\partial \mathrm{t}} - \bar{H}_{\rm os}^x(0)\frac{\partial H(\mathrm{t})}{\partial \mathrm{t}}\right)(r_{rx}^x - r_{\rm sp}^x) \\ &+ \left(\frac{\partial \bar{H}_{\rm os}^y(\mathrm{t})}{\partial \mathrm{t}} - \bar{H}_{\rm os}^y(0)\frac{\partial H(\mathrm{t})}{\partial \mathrm{t}}\right)(r_{rx}^y - r_{\rm sp}^y) \\ &+ \left(\frac{\partial \bar{H}_{\rm os}^z(\mathrm{t})}{\partial \mathrm{t}} - \bar{H}_{\rm os}^z(0)\frac{\partial H(\mathrm{t})}{\partial \mathrm{t}}\right)(r_{rx}^z - r_{\rm sp}^z)\Bigg] \\ &+ h^{-\frac{3}{2}}\left(\frac{\partial \bar{H}_{\rm os}^y(\mathrm{t})}{\partial \mathrm{t}} - \bar{H}_{\rm os}^y(0)\frac{\partial H(\mathrm{t})}{\partial \mathrm{t}}\right)\Bigg\},\end{aligned} \tag{B-7b}$$

$$\frac{\partial H_2^z}{\partial t} = \frac{1}{4\pi}\left(\left[\int_0^t \left\{-3h^{-\frac{5}{2}}\left(r_{rx}^z - r_{\rm sp}^z - \frac{2(t-\mathrm{T})}{\mu_o\sigma s}\right)\right.\right.$$
$$\times\left[\frac{\partial M_x}{\partial t}(r_{rx}^x - r_{\rm sp}^x) + \frac{\partial M_y}{\partial t}(r_{rx}^y - r_{\rm sp}^y)\right.$$
$$\left.+\frac{\partial M_z}{\partial t}\left(r_{rx}^z - r_{\rm sp}^z - \frac{2(t-\mathrm{T})}{\mu_o\sigma s}\right)\right]h^{-\frac{3}{2}}\frac{\partial M_z}{\partial t}\Bigg\}$$
$$-\left\{-\frac{15M_x}{2}h^{-\frac{7}{2}}(r_{rx}^x - r_{\rm sp}^x)\left(r_{rx}^z - r_{\rm sp}^z - \frac{2(t-\mathrm{T})}{\mu_o\sigma s}\right)\frac{\partial h}{\partial t}\right.$$
$$-\frac{3M_x}{2}h^{-\frac{5}{2}}(r_{rx}^x - r_{\rm sp}^x)\frac{4}{\mu_o\sigma s}$$
$$-\frac{15M_y}{2}h^{-\frac{7}{2}}(r_{rx}^y - r_{\rm sp}^y)\left(r_{rx}^z - r_{\rm sp}^z - \frac{2(t-\mathrm{T})}{\mu_o\sigma s}\right)\frac{\partial h}{\partial t}$$
$$-\frac{3M_y}{2}h^{-\frac{5}{2}}(r_{rx}^y - r_{\rm sp}^y)\frac{4}{\mu_o\sigma s}$$
$$-\frac{15M_z}{2}h^{-\frac{7}{2}}\left(r_{rx}^z - r_{\rm sp}^z - \frac{2(t-\mathrm{T})}{\mu_o\sigma s}\right)^2\frac{\partial h}{\partial t} - \frac{3M_z}{2}h^{-\frac{5}{2}}$$
$$\times\left(r_{rx}^z - r_{\rm sp}^z - \frac{2(t-\mathrm{T})}{\mu_o\sigma s}\right)\frac{4}{\mu_o\sigma s}$$
$$\left.-\frac{6}{\mu_o\sigma s}h^{-\frac{5}{2}}\left(r_{rx}^z - r_{\rm sp}^z - \frac{2(t-\mathrm{T})}{\mu_o\sigma s}\right)\right\}d\mathrm{T}\Bigg]\Bigg)$$
$$+\frac{1}{4\pi}\left\{-3h^{-\frac{5}{2}}\left(r_{rx}^z - r_{\rm sp}^z - \frac{2(t-\mathrm{T})}{\mu_o\sigma s}\right)\right.$$
$$\times\left[\left(\frac{\partial \bar{H}_{\rm os}^x(\mathrm{t})}{\partial \mathrm{t}} - \bar{H}_{\rm os}^x(0)\frac{\partial H(\mathrm{t})}{\partial \mathrm{t}}\right)(r_{rx}^x - r_{\rm sp}^x)\right.$$
$$+\left(\frac{\partial \bar{H}_{\rm os}^y(\mathrm{t})}{\partial \mathrm{t}} - \bar{H}_{\rm os}^y(0)\frac{\partial H(\mathrm{t})}{\partial \mathrm{t}}\right)(r_{rx}^y - r_{\rm sp}^y)$$
$$\left.+\left(\frac{\partial \bar{H}_{\rm os}^z(\mathrm{t})}{\partial \mathrm{t}} - \bar{H}_{\rm os}^z(0)\frac{\partial H(\mathrm{t})}{\partial \mathrm{t}}\right)(r_{rx}^z - r_{\rm sp}^z)\right]$$
$$\left.+h^{-\frac{3}{2}}\left(\frac{\partial \bar{H}_{\rm os}^z(\mathrm{t})}{\partial \mathrm{t}} - \bar{H}_{\rm os}^z(0)\frac{\partial H(\mathrm{t})}{\partial \mathrm{t}}\right)\right\}. \qquad \text{(B-7c)}$$

REFERENCES

Abramowitz, M., and I. A. Stegun, 1965, Handbook of mathematical functions: Dover Publications.

Annan, A. P., 1974, The equivalent source method for electromagnetic scattering analysis and its geophysical application: Ph.D. thesis, Memorial University of Newfoundland.

Ayoub, R., 1974, Euler and the Zeta function: The American Mathematical Monthly, **81**, 1067–1086, doi: 10.2307/2319041.

Bartel, D. C., and A. Becker, 1988, Time-domain electromagnetic detection of a hidden target: Geophysics, **53**, 537–545, doi: 10.1190/1.1442485.

Desmarais, J. K., and R. S. Smith, 2015a, Survey design to maximize the volume of exploration of the InfiniTEM system when looking for discrete targets: Journal of Applied Geophysics, **115**, 11–23, doi: 10.1016/j.jappgeo.2015.02.012.

Desmarais, J. K., and R. S. Smith, 2015b, Combining spatial components and Hilbert transforms to interpret ground-time-domain electromagnetic data: Geophysics, **80**, no. 4, E237–E246, doi: 10.1190/geo2014-0528.1.

Desmarais, J. K., and R. S. Smith, 2015c, The total component (or vector magnitude) and the Energy Envelope as tools to interpret airborne electromagnetic data: A comparative study: Journal of Applied Geophysics, **121**, 116–127, doi: 10.1016/j.jappgeo.2015.07.015.

Desmarais, J. K., and R. S. Smith, 2016, Decomposing the electromagnetic response of magnetic dipoles to determine the geometric parameters of a dipole conductor: Exploration Geophysics, **47**, 13–23, doi: 10.1071/EG14070.

Dyck, A. V., M. Bloore, and M. A. Vallée, 1981, User manual for programs PLATE and SPHERE: Research in Applied Geophysics: Geophysics Laboratory Department of Physics, University of Toronto, **14**.

Dyck, A. V., and G. F. West, 1984, The role of simple computer models in interpretations of wide-band, drill-hole electromagnetic surveys in mineral exploration: Geophysics, **49**, 957–980, doi: 10.1190/1.1441741.

Fullagar, P. K., G. A. Pears, J. E. Reid, and R. Schaa, 2015, Rapid approximate inversion of airborne TEM: Exploration Geophysics, **46**, 112–117, doi: 10.1071/EG14046.

Grant, F., and G. West, 1965, Interpretation theory in applied geophysics: McGraw-Hill Book Co.

Lamontagne, Y., J. Macnae, and B. Polzer, 1988, Multiple conductor modeling using program MultiLOOP: 58th Annual International Meeting, SEG, Expanded Abstracts, 237–240, doi: 10.1190/1.1892248.

Lee, T., 1975, Transient electromagnetic response of a sphere in a layered medium: Geophysical Prospecting, **23**, 492–512, doi: 10.1111/j.1365-2478.1975.tb01544.x.

Lee, T., 1983, The transient electromagnetic response of a conducting sphere in an imperfectly conduction half-space: Geophysical Prospecting, **31**, 766–781, doi: 10.1111/j.1365-2478.1983.tb01084.x.

Liu, G., and M. W. Asten, 1993, Fast approximate solutions of transient EM response to a target buried beneath a conductive overburden: Geophysics, **58**, 810–817, doi: 10.1190/1.1443466.

Macnae, J., 2015, 3D-spectral CDIs: A fast alternative to 3D inversion?: Exploration Geophysics, **46**, 12–18, doi: 10.1071/EG14036.

Macnae, J., A. King, N. Stolz, A. Osmakoff, and A. Blaha, 1998, Fast AEM data processing and inversion: Exploration Geophysics, **29**, 163–169, doi: 10.1071/EG998163.

Newman, G. A., and G. W. Hohmann, 1988, Transient electromagnetic responses of high-contrast prisms in a layered earth: Geophysics, **53**, 691–706, doi: 10.1190/1.1442503.

Raiche, A., and F. Sugeng, 1989, Predicting the transient EM response of complex structures using the compact finite-element method: Exploration Geophysics, **20**, 51–55, doi: 10.1071/EG989051.

Reid, J., A. Fitzpatrick, and K. Godber, 2010, An overview of the SkyTEM airborne EM system with Australian examples: Preview, **145**, 26–37, doi: 10.1071/PVv2010n145p26.

San Filipo, B., and I. J. Won, 2005, Broadband electromagnetic detection and discrimination of underwater UXO: Strategic Environmental Research and Development Program, Reports MR-1321, https://www.serdp-estcp.org/Program-Areas/Munitions-Response/Underwater-Environments/MR-1321, accessed 8 February 2016.

Schaa, R., 2010, Rapid approximate 3D inversion of TEM data: Ph.D. thesis, University of Tasmania.

Shubitidze, F., 2011, EMI modelling for UXO detection and discrimination underwater: Strategic Environmental Research and Development Program, Report MR-1632, %%https://www.serdp-estcp.org/Program-Areas/Munitions-Response/Underwater-Environments/MR-1632/MR-1632/%28language%29/eng-US, accessed 8 February 2016.

Singh, S. K., 1973, Electromagnetic transient response of a conducting sphere embedded in a conductive medium: Geophysics, **38**, 864–893, doi: 10.1190/1.1440381.

Smith, R. S., and T. J. Lee, 2001, The impulse-response moments of a conductive sphere in a uniform field, a versatile and efficient electromagnetic model: Exploration Geophysics, **32**, 113–118, doi: 10.1071/EG01113.

Smith, R. S., and T. J. Lee, 2002, The moments of the impulse response: A new paradigm for the interpretation of transient electromagnetic data: Geophysics, **67**, 1095–1103, doi: 10.1190/1.1500370.

Smith, R. S., and B. Neil, 2013, Precision requirements for specifying transmitter waveforms used for modelling the off-time electromagnetic response: Exploration Geophysics, **44**, 1–5, doi: 10.1071/EG12040.

Smith, R. S., and A. S. Salem, 2007, A discrete conductor transformation of airborne electromagnetic data: Near Surface Geophysics, **5**, 87–95, doi: 10.3997/1873-0604.2006021.

Smith, R. S., and R. Wasylechko, 2012, Sensitivity cross-sections in airborne electromagnetic methods using discrete conductors: Exploration Geophysics, **43**, 95–103, doi: 10.1071/EG11048.

Song, J., 1993, Scattering of arbitrarily-polarized EM waves by a discontinuity in a grounded dielectric sheet and propagation of EM pulses excited by an electric dipole in conducting media: Ph.D. thesis, Department of Electrical Engineering, Michigan State University.

Vallée, M. A., and R. S. Smith, 2009, Inversion of airborne time-domain electromagnetic data to a 1D structure using lateral constraints: Near Surface Geophysics, **7**, 63–71, doi: 10.3997/1873-0604.2008035.

Vallée, M. A., 2015, New developments in AEM discrete conductor modelling and inversion: Exploration Geophysics, **46**, 97–111, doi: 10.1071/EG14025.

Wait, J. R., 1953, A transient magnetic dipole source in a dissipative medium: Journal of Applied Physics, **24**, 341–343, doi: 10.1063/1.1721276.
Walker, P. W., and G. F. West, 1991, A robust integral equation solution for electromagnetic scattering by a thin plate in conductive media: Geophysics, **56**, 1140–1152, doi: 10.1190/1.1443133.
Ward, S. H., and G. W. Hohmann, 1987, Electromagnetic theory for geophysical applications, *in* M. N. Nabighian, ed., Electromagnetic methods in applied geophysics: Volume 1, theory: SEG Books, 131–311.
Watson, G. N., 1944, A treatise on the theory of Bessel function: Cambridge University Press.
Witherly, K., R. Irvine, and M. Godbout, 2004, Reid Mahaffy Test Site, Ontario Canada: An example of benchmarking in airborne geophysics: 74th Annual International Meeting, SEG, Expanded Abstracts, 1202–1204.
Wolfgram, P., M. Hyde, and S. Thompson, 1998, How to find localized conductors in GEOTEM data: Exploration Geophysics, **29**, 665–670, doi: 10.1071/EG998665.
Xie, X., J. Macnae, and J. Reid, 1998, The limitations of 1-D inversion for 2-D overburden structures: 68th Annual International Meeting, SEG, Expanded Abstracts, 760–763.